Journal of Solid State Chemistry 184 (2011) 2306–2314

Contents lists available at ScienceDirect

Journal of Solid State Chemistry

journal homepage: www.elsevier.com/locate/jssc

Synthesis and oxygen content dependent properties of hexagonal $DyMnO_{3+\delta}$

S. Remsen [a,*], B. Dabrowski [a,b], O. Chmaissem [a,b], J. Mais [a], A. Szewczyk [c]

[a] Department of Physics, Northern Illinois University, DeKalb, IL 60115, USA
[b] Materials Science Division, Argonne National Laboratory, Argonne, IL 60439, USA
[c] Institute of Physics, Polish Academy of Sciences, Al. Lotników 32/46, 02-668 Warsaw, Poland

ARTICLE INFO

Article history:
Received 28 January 2011
Received in revised form
23 June 2011
Accepted 26 June 2011
Available online 1 July 2011

Keywords:
Hexagonal manganites
Structural properties
Thermal expansion
Chemical expansion
Non-stoichiometric oxygen content

ABSTRACT

Oxygen deficient polycrystalline samples of hexagonal $P6_3cm$ (space group #185) $DyMnO_{3+\delta}$ ($\delta<0$) were synthesized in Ar by intentional decomposition of its perovskite phase obtained in air. The relative stability of these phases is in accord with our previous studies of the temperature and oxygen vacancy dependent tolerance factor. Thermogravimetric measurements have shown that hexagonal samples of $DyMnO_{3+\delta}$ ($0\le\delta\le0.4$) exhibit unusually large excess oxygen content, which readily incorporates on heating near 300 °C in various partial-pressures of oxygen atmospheres. Neutron and synchrotron diffraction data show the presence of two new structural phases at $\delta\approx0.25$ (Hex_2) and $\delta\approx0.40$ (Hex_3). Rietveld refinements of the Hex_2 phase strongly suggest it is well modeled by the $R3$ space group (#146). These phases were observed to transform back to $P6_3cm$ above ~350 °C when material becomes stoichiometric in oxygen content ($\delta=0$). Chemical expansion of the crystal lattice corresponding to these large changes of oxygen was found to be 3.48×10^{-2} mol^{-1}. Thermal expansion of stoichiometric phases were determined to be 11.6×10^{-6} and 2.1×10^{-6} K^{-1} for the $P6_3cm$ and Hex_2 phases, respectively. Our measurements also indicate that the oxygen non-stoichiometry of hexagonal $RMnO_{3+\delta}$ materials may have important influence on their multiferroic properties.

1. Introduction

Structural and physical properties of rare-earth manganites have been studied for over 50 years [1]. Fig. 1 shows schematic drawings of reported perovskite and hexagonal crystal structures and electronic occupation of the 3*d* orbitals in their respective MnO_n polyhedrons. The perovskite orthorhombic *Pnma* structure is based on a three dimensional network of corner shared MnO_6 octahedra. Distortion from the cubic structure, which can be explained by the low value of the tolerance factor ($t=(R-O)/\sqrt{2}(Mn-O)<1$), is due to the difference in the (R–O) and (Mn–O) bond lengths. Furthermore, Jahn–Teller distortion of the MnO_6 octahedra, which is caused by the two-fold degeneracy of the Mn^{3+} ion in a high-spin state of t^3e^1, results in the elongated *c*-axis and three different (Mn–O) bond lengths [2]. These distortions shift and rotate the octahedra along the *ab* plane and tilt and rotate the octahedra about the *c*-axis, which results in considerably smaller than 180° Mn–O–Mn bond angles that has large impact on the transport and magnetic properties of the system [3,4]. The non-centrosymmetric hexagonal $P6_3cm$ structure can be described as close-packed layers of trigonal bipyramids of MnO_5, which are centered at Mn^{3+} sites and are separated by layers of R^{3+} ions. The MnO_5 bipyramids are rotated in the *ab* plane (planar bond angles Mn–O–Mn $\neq180°$) and tilted relative to the *c*-axis due to the difference of the (R–O) and (Mn–O) bond lengths [5]. However, unlike in the MnO_6 octahedra, high-spin Mn^{3+} ions in the MnO_5 bipyramids are not Jahn–Teller active.

Recently, hexagonal manganites have been the subject of much investigation due to the rare coexistence of antiferromagnetic ordering and ferroelectricity. Long-range magnetic ordering occurs in these materials for both the Mn^{3+} and R^{3+} ions at $T_N\sim70$–130 and ~5–10 K, respectively. A spin rotation transition of the Mn^{3+} ions has also been reported between these two temperatures at ~40–60 K. $RMnO_3$ materials are ferroelectric below a high Curie temperature of $T_c\sim300$–650 °C [5–13]. Magnetic ordering of Mn^{3+} and Dy^{3+} for $DyMnO_3$ has been reported for single crystal and polycrystalline samples at $T_N\sim70$–80 and ~3–8 K, respectively [13–17]. To the best of our knowledge, elevated temperature studies of the hexagonal $DyMnO_3$ phase are currently limited to synthesis techniques.

Conventionally, the formation of the perovskite versus hexagonal phase is governed primarily by the size of the rare-earth ion in $RMnO_3$ (with constant Mn^{3+} size). During high-temperature solid state synthesis in air, the perovskite phase forms easily with larger rare-earth elements (e.g. La, Pr, Nd, Sm, Gd, Tb, and Dy), while smaller size rare-earths (e.g. Ho, Er, Tm, Yb, Lu, and Y) favor the hexagonal phase. It has been observed that the perovskite structure is stable for a tolerance factor (calculated at room temperature

* Corresponding author. Fax: +1 815 753 8565.
E-mail address: sremsen@gmail.com (S. Remsen).

0022-4596/$ - see front matter © 2011 Elsevier Inc. All rights reserved.
doi:10.1016/j.jssc.2011.06.037

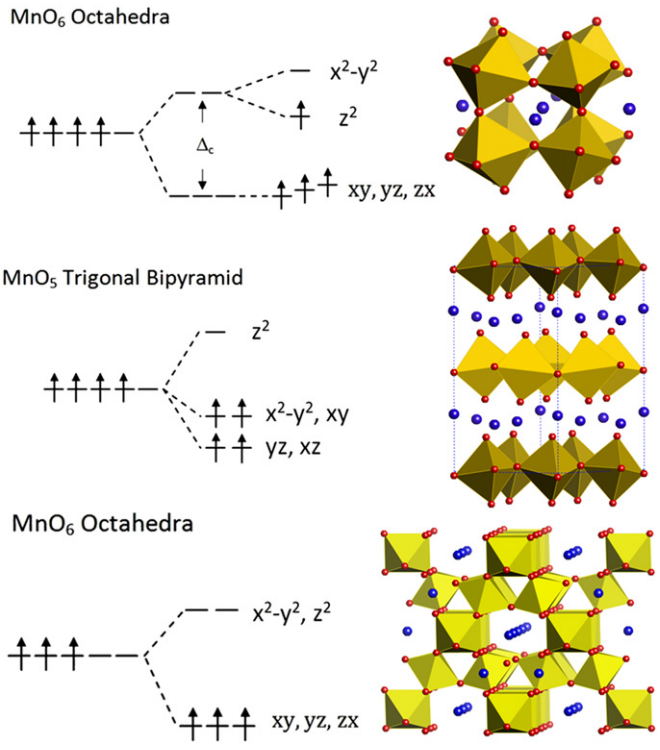

Fig. 1. Schematic drawings of the crystal structures and 3*d* orbitals of orthorhombic perovskite *Pnma* (top), hexagonal $P6_3cm$ (middle), and pyrochlore *Fd*3*m* (bottom) where red spheres, yellow polyhedrons, and blue spheres represent O^{2-} anions, MnO_n polyhedrons, and R^{3+} cations, respectively (all figures, only Dy^{3+} cations and MnO_n polyhedrons are displayed).

using Shannon's values [14,18]) in the range of $0.855 \leq t \leq 1$ [19], whereas the hexagonal phase is stable for $t < 0.855$ [20]. Recently, Zhou et al. [6] suggested that the relative large difference in density between the perovskite and hexagonal phases may have a large impact on the formation of the perovskite versus the hexagonal structure near the lower limit of the tolerance factor. $DyMnO_3$ has a tolerance factor of 0.857 at room temperature [14,18] and will tend to form the perovskite phase under normal solid state synthesis in air. Hydrothermal synthesis in 3 kbar at 500 °C has also been shown to favor the oxidation state of Mn^{4+}, which results in the formation of the $Dy_2Mn_2O_7$ pyrochlore *Fd*3*m* phase (see Fig. 1) [21]. Octahedral coordinated Mn^{4+} is not a Jahn–Teller ion, therefore the MnO_6 octahedra in the pyrochlore phase are not subject to the same distortions as in the perovskite phase.

Our work here describes the synthesis of hexagonal $DyMnO_3$ by decomposition of the perovskite phase in Ar, which was guided by our previous work on the temperature and oxygen vacancy dependence of the tolerance factor of manganites [22]. Thermogravimetric measurements of oxygen annealed hexagonal samples indicated unusually large changes of oxygen content over a narrow temperature range near 300 °C. Preliminary structural studies with neutron and X-ray powder diffraction (NPD and XRD) have revealed two new $DyMnO_{3+\delta}$ hexagonal phases. These results indicate the hexagonal family of $RMnO_3$ is prone to considerable oxygen non-stoichiometry. The chemical expansion properties resulting from these large changes in oxygen are also reported, as well as the thermal expansion coefficient of stable oxygen content regions.

2. Experimental techniques

Synthesis was done by solid state reaction, which is further detailed in the following section. XRD measurements were made with a Rigaku D/MAX powder diffractometer in the $2\theta = 20$–70° range with Cu*K*α radiation. Time-of-flight NPD measurements were conducted at Argonne National Laboratory's former Special Environment Powder Diffractometer (SEPD) at the Intense Pulsed Neutron Source (IPNS). High resolution synchrotron X-ray data were collected at room temperature with a wavelength of 0.40225 Å at the Advanced Photon Source of Argonne National Laboratory (beamline 11BM-B). The sample for synchrotron measurement was loaded in a fine glass capillary and made to spin during the experiment to eliminate possible undesired texturing or preferred orientation effects. Structural refinements were performed by the Rietveld method with GSAS/EXPGUI suite programs [23]. Thermogravimetric analysis (TGA) measurements were made with Cahn TG171 and Cahn TherMax700 thermobalances in several different partial-pressures of oxygen and hydrogen (balanced with argon) up to 1400 °C with heating and cooling rates of 0.1–1.0°/min. TGA samples were approximately 1 g and were measured with a 5 μg precision. Dilatometry measurements were made with a Linseis Differential Dilatometer L75 and samples were measured with a 1 μm precision.

3. Results and discussion

3.1. Synthesis, stability, and oxygen content

Polycrystalline samples of $DyMnO_{3+\delta}$ were synthesized by solid state reaction with appropriate amounts of Dy_2O_3 and MnO_2 (both with > 99.99% purity). For all samples, reactants were thoroughly mixed in an agate mortar, and fired in air in the temperature range 800–1200 °C with intermediate grindings followed by pressing samples into high-density pellets at approximately 10 kbar. All steps of the synthesis were monitored with XRD measurements. Samples were fired several times in air until the single phase perovskite structure was obtained. The hexagonal phase was acquired from perovskite sample by firing under ultra-high-purity argon (99.999%) with a hydroxyl purifier (measured oxygen partial-pressures of 5–10 ppm) at 1400 °C. Part of the hexagonal sample was then annealed at 500 °C in TGA with 0.1 °C/min heating and cooling in 21% O_2/Ar (Fig. 2, curve 1). The oxygen contents after initial synthesis and of the following annealing were then determined with TGA by the difference in weight between this oxygenated sample ($\delta = 0.21$) and its reduction products, Dy_2O_3 and MnO (verified by XRD), obtained by slow reduction at 0.1 °C/min in 42% H_2/Ar (Fig. 2, curve 2); thus, Fig. 2 is normalized to its reduction products ($\delta = -0.5$).

Considerable effort was devoted to synthesizing homogenous hexagonal samples. Hexagonal $DyMnO_3$ has been previously achieved by epitaxially stabilized crystal growth with thin-films [16], thermal decomposition with polynuclear coordination compound precursors [24], quenching methods from 1600 °C in air [25], or firing at 1250 °C in argon for 3 days with sol–gel methods [17]. Our work confirmed that synthesis in low partial-pressures of oxygen at high-temperature tends to favor the formation of the hexagonal phase, while synthesis in oxygen tends to favor the perovskite phase [26]. The oxygen content dependence of the tolerance factor, which we have previously studied for substituted $SrMnO_3$ [22], is most likely responsible for this behavior. The formation of oxygen vacancies ($\delta < 0$) in $RMnO_{3+\delta}$ causes a change in oxidation state in some of the Mn^{3+} cations to Mn^{2+}, resulting in a net $Mn^{(3+2\delta)+}$ cation, which increases the (Mn–O) bond length with decreasing values of δ [18]. Thermogravimetric measurements (curve 1, Fig. 2) show this reduced starting oxygen content of $\delta \approx -0.037$. The resulting larger (Mn–O) bond lengths decrease the tolerance factor below the lower limit of 0.855 and results in the perovskite structure undergoing a phase transition to the hexagonal phase. Using Shannon's room temperature ionic

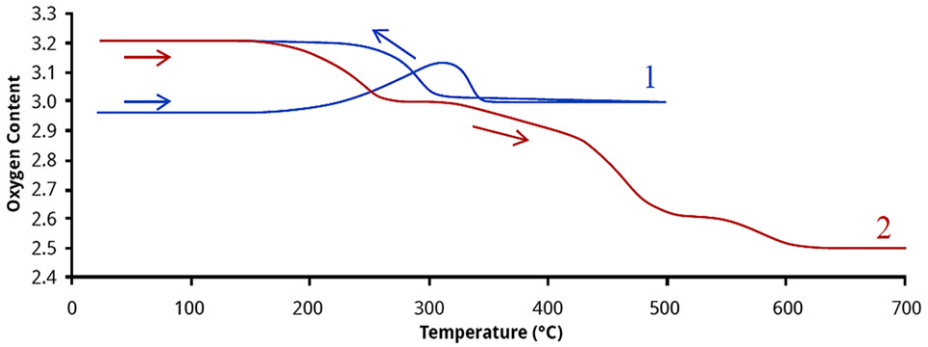

Fig. 2. TGA annealing in 21% O_2 after initial synthesis in argon (curve 1) and subsequent reduction of $DyMnO_{3+\delta}$ in 42% H_2 to Dy_2O_3 and MnO (curve 2).

size values, $DyMnO_{3+\delta}$ needs $\delta = -0.023$ to have $t \leq 0.855$. We have observed, however, that samples with such δ did not transform completely to the hexagonal phase at 1400 °C. Our previous in situ measurements with Ca and La substituted $SrMnO_3$ [22,27] have shown that both (Ca,Sr,La–O) and (Mn–O) bond lengths increase with temperature in a manner which increases the value of the tolerance factor. Therefore the transition from the perovskite to the hexagonal phase will most likely occur in various oxygen pressures at δ which is a function of temperature, for example, in ~10 ppm O_2 at 1400 °C as we observed here or in air at 1600 °C as previously reported [25]. Further high-temperature in situ NPD would be needed to fully substantiate this assertion. This transition may be also enhanced by the difficultly of maintaining the 12-fold coordination of R required for the perovskite phase in an oxygen deficient atmosphere at high-temperatures; thus, an eight-fold coordination with hexagonal symmetry results. Whatever the case, the reducing conditions needed for production of bulk polycrystalline samples of hexagonal $P6_3cm$ $DyMnO_{3+\delta}$ by standard firing methods were very near to decomposition to simple oxides and many attempts were needed to find the most favorable temperature and time of the firings. Hexagonal $DyMnO_3$ was also observed with TGA measurements (Fig. 2, confirmed with XRD) to remain stoichiometric in oxygen above ~350 °C, begin slight decomposition back to the perovskite phase at 1100 °C and completely transform to the perovskite phase at 1400 °C, which is in agreement with the presented tolerance factor arguments.

To study oxygen enriched hexagonal phases, samples were annealed after initial synthesis in varying conditions to achieve a larger range of oxygen contents ($\delta \geq 0$). The oxygen content behavior during annealing in oxygen (TGA, curve 1 of Fig. 2) shows $DyMnO_{3+\delta}$ to be stoichiometric ($\delta \approx 0$) above 350 °C. Using this information, a stoichiometric sample was synthesized by quenching a sample from air at 420 °C to liquid nitrogen (verified by change in weight). Samples with $\delta > 0$ were obtained on TGA by heating to 400–500 °C and slow cooling to room temperature at 0.1–1.0 °C/min in 21–100% O_2 at ambient pressure. The final oxygen content of these samples was determined by normalizing to stable weights above 400 °C. A high-pressure oxygen annealing at 400 °C followed by 0.1 °C/min cooling in 250 bars of O_2 was also used to synthesize a sample with high oxygen content. The oxygen content of this sample was studied with TGA (1 °C/min heating) in 21% O_2 by normalizing to $\delta = 0$ at 375 °C (Fig. 3). TGA data also shows an enhanced stability on reduction near a temperature of 300 °C and an oxygen content of $\delta \approx 0.25$, which suggests the existence of a stable phase at $DyMn^{3+}_{0.5}Mn^{4+}_{0.5}O_{3.25}$ and, possibly, the presence of another stable phase at or above an oxygen content of 3.35. Table 1 is a compilation of synthesis conditions used after formation of the $P6_3cm$ phase and the oxygen contents of these annealed samples.

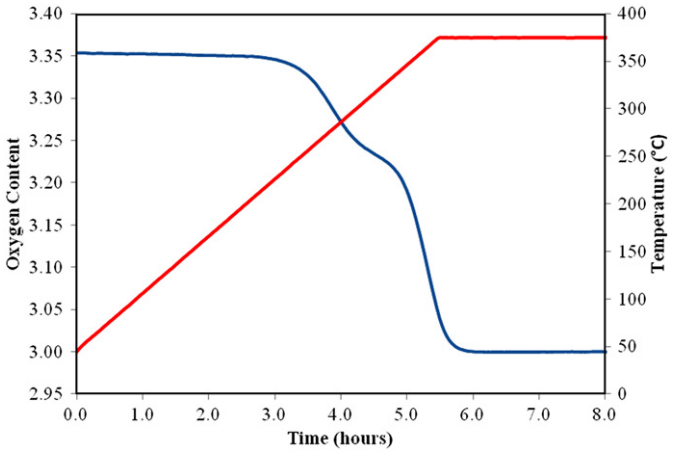

Fig. 3. TGA reduction in 21% O_2 of high-pressure annealed $DyMnO_{3+\delta}$ to stable 3.0 oxygen content.

To the best of our knowledge, the large increases in oxygen content of hexagonal $DyMnO_{3+\delta}$ observed in TGA during annealings have not been previously reported for any other hexagonal $RMnO_3$ materials, which are generally believed to remain stoichiometric at elevated temperatures in various partial-pressures of oxygen. We have found that large oxygen non-stoichiometry is not unique for $DyMnO_{3+\delta}$ [28] and, as will be shown in the next section, results in new hexagonal structures. This behavior may not have been previously observed for other hexagonal manganites due to the narrow range of temperatures (~200–350 °C) where these new phases exist upon heating before returning back to the $P6_3cm$ structure with $\delta = 0$ above ~350 °C, and the high oxygen partial-pressures they require on slow cooling. As discussed in the introduction, this temperature range has not been of particular interest for structural studies of $RMnO_3$, as most previous work has been done at either low-temperature to study magnetic ordering (≤ 200 K) or high-temperatures to measure the rattling behavior of the MnO_5 bipyramids or structural transitions (≥ 500 °C). If large oxygen non-stoichiometry is present for all hexagonal manganites, since most preparation methods of these samples use high-temperature synthesis (≥ 1000 °C) followed by cooling in air, typical samples may contain varying amounts of excess oxygen content. We have previously observed that small oxygen non-stoichiometry in perovskite manganites can have profound effects on their magnetic and transport properties [29,30], and this could very well have a large impact on the multiferroic properties of the hexagonal system. In the following sections we will show that this effect has a considerable impact on the structural and thermal/chemical expansion properties of $DyMnO_{3+\delta}$.

Table 1
List of annealed $DyMnO_{3+\delta}$ samples.

Sample no.	Conditions after synthesis of $P6_3cm$ in Ar	Sample type	δ
1	None	Small pellets	−0.037
2	Quenched from 420 °C air	Small pellets	0.00
3	Cooled from 500° at 1.0 °C/min in 21% O_2 at standard pressure	Small pellets	0.18
4	Cooled from 500° at 1.0 °C/min in O_2 at standard pressure	Small pellets	0.21
5	Cooled from 500° at 0.1 °C/min in O_2 at standard pressure	Small pellets	0.24
6	Cooled from 500° at 0.1 °C/min in O_2 at ~250 bars	Small pellets	0.35

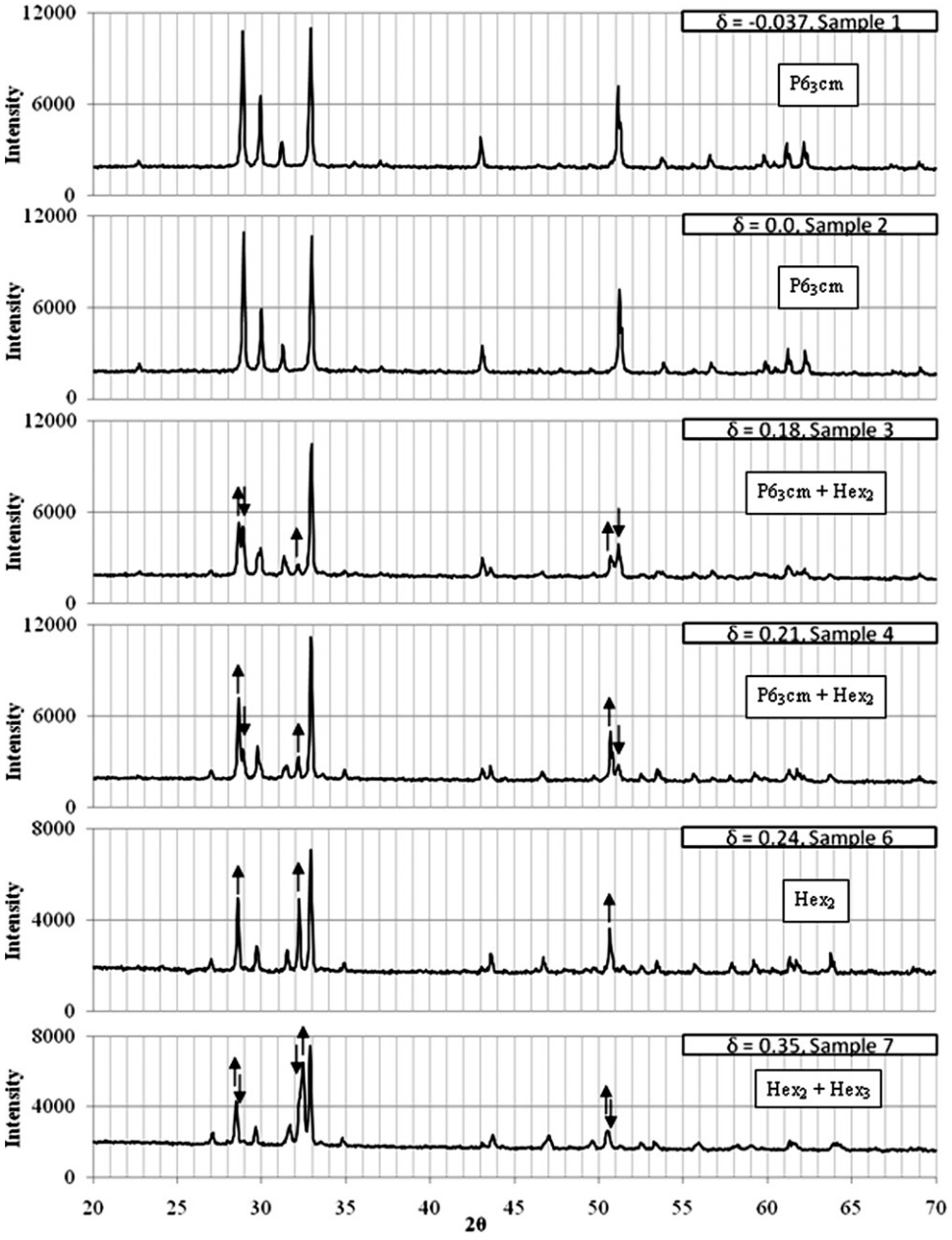

Fig. 4. XRD patterns of $DyMnO_{3+\delta}$, with $\delta = -0.037$, 0.0, 0.18, 0.21, 0.24, and 0.35. Arrows indicate the increase (↑) and decrease (↓) of peak intensity for the various hexagonal phases.

3.2. Crystal structure

XRD measurements were made to verify the hexagonal $P6_3cm$ structure of $DyMnO_{2.963}$ and $DyMnO_{3.0}$ (samples 1 and 2) and to obtain a preliminary structural understanding of annealed samples. Fig. 4 is a compilation of XRD patterns collected for samples 1–4, 6, and 7 shown in Table 1. Peak positions and intensities of $DyMnO_{2.963}$ and $DyMnO_{3.0}$ were found to be in good agreement with previously reported XRD patterns of $P6_3cm$ $DyMnO_3$ [17]. Furthermore, XRD data of the quenched sample

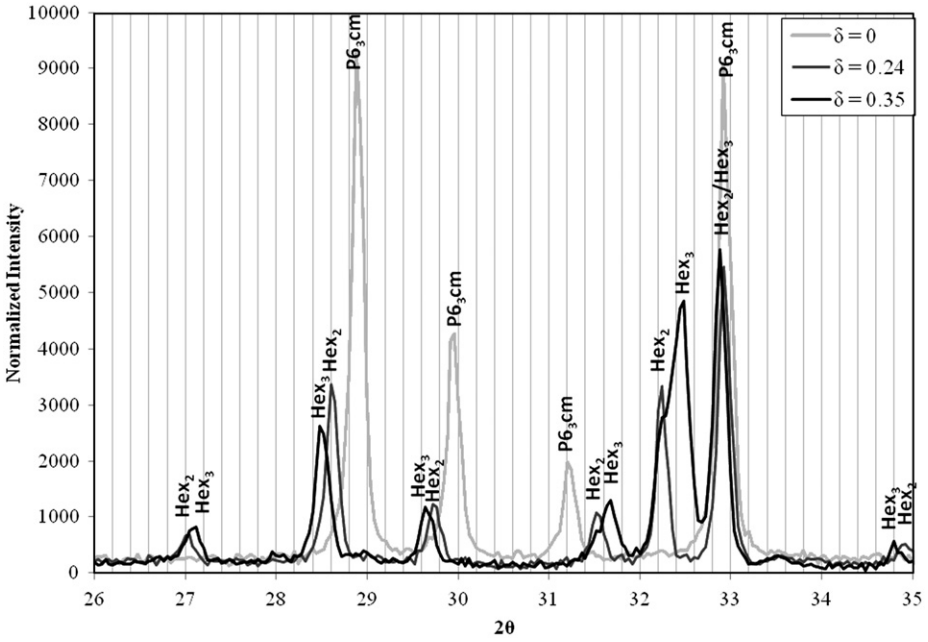

Fig. 5. XRD comparison of $DyMnO_{3+\delta}$ samples: $P6_3cm$ ($\delta=0$), nearly single phase Hex_2 ($\delta=0.24$) and mixed phase of Hex_2 and Hex_3 ($\delta=0.35$).

(sample 2) confirmed that stoichiometric samples are indeed the hexagonal $P6_3cm$ phase after quenching from above 400 °C as observed with TGA data. XRD patterns of annealed samples (samples 3, 4, and 6) in the δ range 0.18–0.24 clearly show growth of a second phase (Hex_2) and a disappearance of the $P6_3cm$ phase (where arrows indicate the growth and decrease of selected peaks for the $P6_3cm$ and the Hex_2 phase, respectively). The diffraction pattern of sample 6 ($\delta=0.24$) is nearly single phase for this new set of peaks and is in agreement with the stability seen in TGA at $\delta\sim0.25$ (Fig. 3). Finally, the XRD pattern of the high-pressure annealed sample (sample 7, $\delta=0.35$) shows a decrease of peak intensity for the Hex_2 phase and the presence of additional peaks (third phase, Hex_3), which is again in agreement with TGA observations. The relative intensities of the Hex_2 and Hex_3 phases suggest that the Hex_3 phase could have an oxygen content of $\delta\approx0.40$, though this is difficult to approximate due to the high degree of peak position overlapping. To help clarify the development of new peaks and peak overlap, Fig. 5 shows an overlay of XRD patterns of samples 2, 6, and 7 ($\delta=0.0$, 0.24, and 0.35) in the 2θ range 26–35°. Figs. 4 and 5 show similarities of the diffraction patterns of the Hex_2, Hex_3, and $P6_3cm$ phases, which suggest that the Hex_2 and Hex_3 phases are structurally related to the $P6_3cm$ phase. The increased number of peaks seen in the Hex_2 and Hex_3 phases versus the $P6_3cm$ phase also suggests a general lowering of symmetry or the formation of a superstructure. Finally, it should also be noted, though these transformations are unlikely at these low-temperatures under O_2, that the Hex_2 and Hex_3 phases were compared to patterns of other known $R_xMn_y^{4+}Mn_{y-1}^{3+}O_{3+\delta}$ systems (e.g. pyrochlore $R_2Mn_2O_7$, perovskite $R-3c$, R_2MnO_4 and RMn_2O_5 phases) and oxides (Mn_2O_3, MnO_2), which could account for the increase in oxygen content. No traces of these structures were observed.

Guided by our initial XRD investigation, NPD measurements were conducted for selected samples. High-resolution, backscattering data ($2\theta=144°$, Bank 1 of SEPD) were used for $DyMnO_{2.963}$, $DyMnO_{3.0}$, and $DyMnO_{3.21}$ (samples 1, 2, and 4, respectively) at room temperature. Low-angle scattering data ($2\theta=44°$, bank 3) were also used for $DyMnO_{3.21}$ at room temperature. High resolution synchrotron X-ray data were also collected for $DyMnO_{3.21}$ at room temperature.

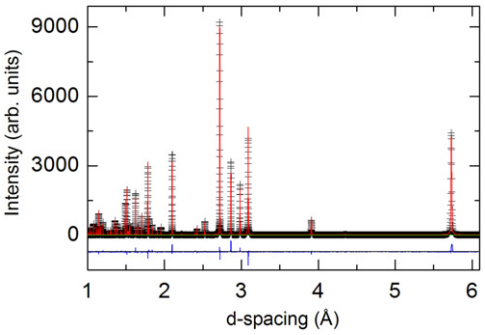

Fig. 6. Example of NPD pattern for $DyMnO_{2.963}$ (SEPD). Plus signs are observed data and the line below is the difference between experimental data and best fit calculated from the Rietveld refinement method.

Raw data for samples 1 and 2 were analyzed with the Rietveld method in the space group $P6_3cm$ based on previous reports for the hexagonal $RMnO_3$ system and our XRD measurements (Fig. 6). Structural sites of this refinement were 2*a* for Dy1 and O3; 4*b* for Dy2 and O4; and 6*c* for Mn1, O1, and O2. Cations occupancies were fixed at one and the site occupancies of oxygen ions were allowed to vary. Initial refinements of the $DyMnO_{3.0}$ sample's occupancies varied less than one standard deviation from fully stoichiometric oxygen content and were fixed to one for its final fitting. For $DyMnO_{2.963}$ occupancies of the O1 and O2 sites were also fixed to one as refinements yielded values slightly greater than one. Oxygen ion vacancies were found to prefer the O3 and O4 sites nearly equally. The resulting oxygen content of this sample calculated from these refined occupancies ($\delta\approx-0.045$) is in reasonable agreement with the value obtained from TGA ($\delta\approx-0.037$). For both these samples (1 and 2), the calculated diffraction pattern of $P6_3cm$ is in good match with the observed data for both samples (Table 2) and their lattice parameters are in agreement with a previous XRD report for $DyMnO_3$ [17]. Bond lengths in Table 2 were calculated using the geometric average [22] by assuming full site occupancy. The average (Mn–O) bond length clearly increases from the stoichiometric to the reduced state, while the average (Dy–O) bond length remains, relatively,

Table 2
Atomic coordinates, lattice parameters, site occupancies, thermal factors, and agreement factors of $P6_3cm$ $DyMnO_{3+\delta}$.

$P6_3cm$		$DyMnO_{3+\delta}$ ($\delta<0$)				
Atom	Position	*X*	*Y*	*Z*	*N*	$U_{iso}\times 100$ (Å^2)
Dy1	2*a*	0	0	0.2794(3)	1	0.559
Dy2	4*b*	0.33	0.67	0.2395(0)	1	0.705
Mn1	6*c*	0.3291(5)	0	0.0055(5)	1	0.388
O1	6*c*	0.3099(9)	0	0.1664(7)	1	0.57[a]
O2	6*c*	0.6440(3)	0	0.3375(6)	1	0.81[a]
O3	2*a*	0	0	0.4874(0)	0.954(4)	0.79[a]
O4	4*b*	0.33	0.67	0.0251(1)	0.954(9)	1.03[a]
$\langle$Dy–O$\rangle_g$ (Å)		2.5509(3)				
$\langle$Mn–O$\rangle_g$ (Å)		1.9971(5)				
Lattice parameters (Å)		a=6.1811(9), c=11.4620(3)				
V (Å^3)		379.250(7)				
Reliability factors		R_p=6.23%, R_{wp}=8.40%, χ^2=2.044				
$P6_3cm$		$DyMnO_{3.0}$				
Atom	Position	*X*	*Y*	*Z*	*N*	$U_{iso}\times 100$ (Å^2)
Dy1	2*a*	0	0	0.2804(7)	1	0.340
Dy2	4*b*	0.33	0.67	0.2392(2)	1	0.415
Mn1	6*c*	0.3310(6)	0	0.0056(2)	1	0.223
O1	6*c*	0.3089(3)	0	0.1688(7)	1	0.75[a]
O2	6*c*	0.6410(4)	0	0.3444(7)	1	0.75[a]
O3	2*a*	0	0	0.4812(1)	1	0.67[a]
O4	4*b*	0.33	0.67	0.0211(3)	1	0.67[a]
$\langle$Dy–O$\rangle_g$ (Å)		2.5515(4)				
$\langle$Mn–O$\rangle_g$ (Å)		1.9835(6)				
Lattice parameters (Å)		a=6.1713(2), c=11.4436(7)				
V (Å^3)		377.443(6)				
Reliability factors		R_p=3.34%, R_{wp}=4.50%, χ^2=3.010				

[a] $D_{eqv.}$

unchanged. Again, this is due to the enlargement of the $Mn^{(3+2\delta)+}$ cation with increasing oxygen deficiency. These results are in agreement with the oxygen vacancy dependence of the tolerance factor and support our synthesis arguments of forming the hexagonal phase by reduction of the perovskite $RMnO_{3+\delta}$ phase.

Analysis of neutron and synchrotron diffraction data for sample 4 ($DyMnO_{3.21}$) revealed the formation of a large superstructure constructed by tripling the *c*-axis of the $P6_3cm$ phase ($c>33$ Å). Several other superstructure models and combinations of possible phase mixtures were also examined but they all failed to index the large number of extra peaks. Analysis of the superstructure's structural symmetry led to the identification of *R*3 as the space group that could successfully index all peaks including the tiny ones. We note here that there is no direct relationship between the two $P6_3cm$ and *R*3 space groups. Such a group/subgroup relationship is not required for two samples that are not chemically the same. A group/subgroup relationship is required when dealing with a unique sample in which structural phase transitions occur at various temperatures or pressures. In the present case, the R3 structure of the oxygen loaded $DyMnO_{3.21}$ sample was determined as the space group of the highest symmetry that can be successfully used to index all Bragg reflections and refine the positions of the Dy and Mn cations. Determination of the exact locations and site occupancies of the diverse oxygen atoms remain challenging due to the complexity of the superstructure and the nature of synchrotron X-rays that are inherently much less sensitive to oxygen than neutrons, especially in the presence of Mn and the heavy Dy rare-earth. Rietveld refinements using synchrotron data are presented in Fig. 7. In the refinements, the cation positions and thermal factors were all refined whereas the oxygen atoms were kept fixed at positions derived from the tripled structure. As shown in the figure, two phases were included in the final refinements: the small parent $P6_3cm$ hexagonal structure (lower tick marks) and the larger *R*3 superstructure (upper tick marks). Fractional

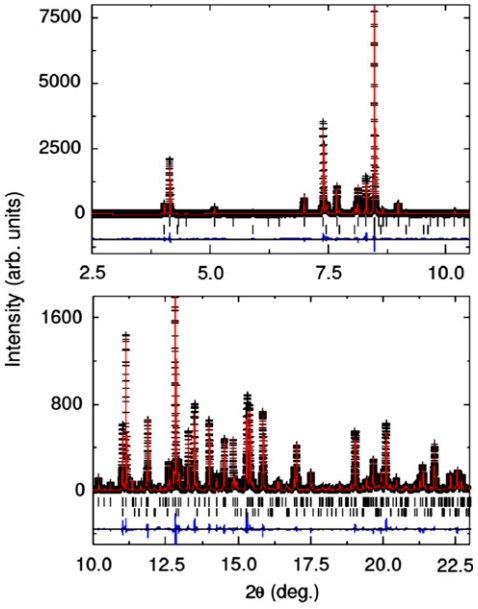

Fig. 7. Best-fit Rietveld refinement patterns using high resolution synchrotron X-ray data with a wavelength of 0.40225 Å (11BM-B). Observed (plus signs) and calculated (solid line) intensities are displayed together with their difference (solid line at the bottom of each panel). Lower and upper tick marks indicate the locations of Bragg reflections for the parent $P6_3cm$ and superstructure *R*3 phases, respectively. Please see the text for details.

percentages by weight for the two phases refined to 14% and 86%, respectively. It is obvious that the parent phase fails to index the observed extra peaks that refine with *R*3. The superstructure's lattice parameters are shown in Table 3 together with the positions of the Dy and Mn cations in which we have high confidence. The exact determination of the oxygen atoms in such a small molecule-like superstructure would necessitate further collection of high quality neutron diffraction data preferably using new $RMnO_{3+d}$ samples in which the highly neutron absorbing Dy would be replaced by Y or other trivalent rare-earth elements with significantly smaller neutron absorption cross sections such as Ho and Er.

3.3. Thermal and chemical expansion

Expansion of the crystal lattice, in both the hexagonal and perovskite $RMnO_3$ phases, can occur through two mechanisms: thermal and chemical expansion. Thermal expansion (TE), as discussed in tolerance factor arguments, is caused by expansion of the (R–O) and (Mn–O) bond lengths due to increased thermal energy at elevated temperature. This effect has been extensively studied with both in situ structural measurements and dilatometry for both the $RMnO_3$ perovskite and hexagonal systems and can have a large impact on their magnetic, transport, and structural properties [4,5,9,10,22,27,31–33]. Chemical expansion (CE) is expansion of the lattice due to changes in oxygen stoichiometry. The effect of CE in the perovskite system has also been heavily studied for changes of structural properties and has great importance on the macro-scale for applications such as films, coatings, and layer materials [34–38]. On the other hand, there are no reports of CE measurements for the hexagonal manganites. It should also be noted that in some cases the thermal expansion coefficient (TEC) is considered to be the net result of both CE and TE; here we consider these to be separate effects, thus TEC in this report is only attributed to TE.

Table 3
Structural parameters for the *R*3 superstructure of $DyMnO_{3.21}$.

*R*3	$DyMnO_{3.21}$			
Atom	*x*	*y*	*z*	*B* (Å^2)
Dy1	0	0	−0.06995(5)	0.30(4)
Dy2	0	0	0.07051(5)	0.04(4)
Dy3	0	0	0.25180(11)	0.19(3)
Dy4	0	0	0.43022(6)	0.97(5)
Dy5	0	0	0.57090(6)	0.50(4)
Dy6	0	0	0.74966(11)	0.32(3)
Mn1	0.4261(5)	0.0019(9)	0	2.8(1)[a]
Mn2	0.3672(7)	0.6254(6)	0.50109(21)	0.47(6)[a]
Lattice parameters (Å)	a=6.231(4) and c=33.346(3)			
Reliability factors	R_{wp}=13.7%, R_p=9.8%, R_I=4.4%, c^2=11.4			

[a] These values clearly correlate with the undetermined distorted oxygen environment around Mn as expected from the insertion of fractional amounts of additional oxygen. Please see the text for more details.

For $RMnO_{3+\delta}$ perovskites measurements of CE typically must be measured separately from TE because both CE and TE change at similar rates as a function of temperature. Oxygen absorption of nominal amounts of δ occurs in the $RMnO_{3+\delta}$ perovskite phase during a *Pnma*—$R-3c$ transition and creates an equal number of *A* and *B* site vacancies, i.e. $R_{1-\nu}Mn_{1-\nu}O_3$ ($\nu \approx \delta/3$), while oxygen remains stoichiometric [39]. These changes in nominal oxygen content are usually relatively small ($\delta \leq 0.15$), and occur slowly over a wide range of temperatures (~500–1000 °C) [4]. Thus, investigations of CE must be done at constant temperature over long lengths of time ($\geq$72 h) with changes in oxygen partial-pressure to change oxygen content and make it possible to separate the effects of TE from CE. However, our TGA measurements for hexagonal $DyMnO_{3+\delta}$ phase have shown large changes in oxygen stoichiometry between two stable oxygen content regions, which occur over a relatively short time scale ($\leq$2 h) and narrow range of temperatures (~100 °C). These characteristics allow us to measure the effective CE over a narrow range temperature by simply subtracting the relatively small value of TE from the observed value of CE. Similarly precise measurements of TE, without the any effect from CE, were possible in temperature regions of stable oxygen content. The following equations were used to calculate TE and CE:

$$\mathrm{TEC} = \frac{1}{L_0}\frac{1}{n-m}\sum_{i=m}^{n}\frac{\Delta L_{i+1}-\Delta L_i}{T_{i+1}-T_i},$$

measured in K^{-1}, where L_0, δL, and T are the sample starting length, the change in length, and temperature, respectively, and m and n are the sets from the measured temperature ranges and

$$\mathrm{CE} = \frac{1}{\Delta\delta}\left(\frac{\Delta L}{L_0} - \langle \mathrm{TEC} \rangle \Delta T\right),$$

measured in (moles of O)$^{-1}$, where $\Delta\delta$ is the absolute change in oxygen content from stoichiometric 3.0 and $\langle$TEC$\rangle$ is the average TEC of the two oxygen content stable regions.

A perovskite sample of $DyMnO_3$ for dilatometry was cut from a dense pellet after initial synthesis in air (~5 × 3 × 2 mm^3 in shape) and was measured in 21% O_2/Ar atmosphere with heating rates of 0.5 °C/min to 900 °C (Fig. 8). Our previous studies of the perovskite $DyMnO_{3+\delta}$ phase have shown that it remains stoichiometric in 21% O_2/Ar up to ~1000 °C [4], thus the expansion seen in Fig. 8 is solely due to TE. The TEC was measured from 50 to 850 °C and was found to be 7.3×10^{-6} K^{-1}, which is in good agreement with a previous report [31].

A pellet of the hexagonal material (~5 × 3 × 2 mm^3 in shape) was also cut from dense sample after initial synthesis and annealed before dilatometry measurement (sample 5). The oxygen

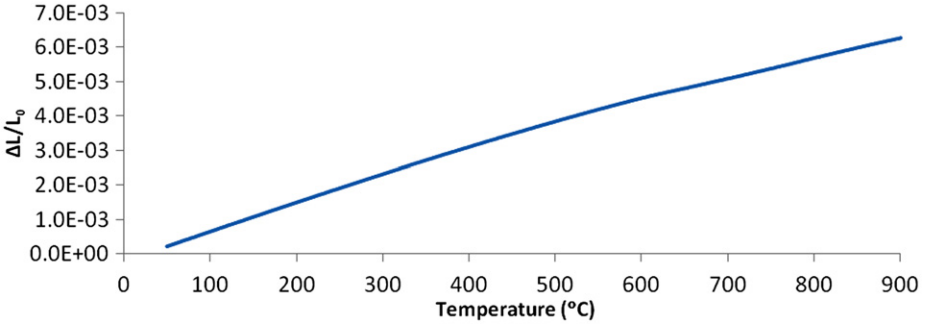

Fig. 8. Dilatometry measurement of perovskite $DyMnO_{3.0}$ in 21% O_2.

content was also measured with identical starting sample and measurement conditions on TGA (Fig. 9a) to determine appropriate temperature ranges to separately extract TE and CE. TE was measured in temperature regions of stable oxygen content observed in TGA of 50–300 °C ("$\delta=0.22$") and 600–850 °C ("$\delta=0$") and the CE for the reduction from $\delta=0.22$ to 0.015 of hexagonal system was also measured in the temperature range 300–380 °C, where approximately 93% of the total oxygen reduction occurs (Fig. 9b). The lower starting oxygen content after annealing in oxygen and the slower reduction of the dense pellet from 390 to 650 °C seen in Fig. 9a when compared to the small chunks of material during TGA measurement shown in Fig. 2 (sample 6) are due to the differences in the samples' density, surface area, and diffusion distances. The TEC of the hexagonal phases in these two temperature regions of stable oxygen content were found to be quite different, $10.2\times10^{-6}\,K^{-1}$ ("$\delta=0.22$"), $2.1\times10^{-6}\,K^{-1}$ ("$\delta=0$"), which indicates the TEC of the Hex_2 phase ($\delta\approx0.25$, assumed) is $\sim11.6\times10^{-6}\,K^{-1}$, and the chemical expansion during the reduction from $\delta=0.22$ to 0.015 is $3.48\times10^{-2}\,mol^{-1}$.

Previous structural and dilatometry reports on single-crystal hexagonal $RMnO_3$ (R=Y, Ho, Sc, and Lu) have shown that lattice parameters linearly increase in-plane and decrease along the c-axis with increasing temperature [5,33]. The contraction along the c-axis has also been shown to increase for larger R ions causing small changes of the unit cell with temperature. Thus, the effect of substantial contraction along the c-axis is most likely responsible for the significantly lower TEC of our polycrystalline $P6_3cm$ material when compared to the Hex_2 and perovskite phases. Increased rate of contraction along the c-axis at the Curie temperature, ~650 °C, was reported previously for $YMnO_3$ and $HoMnO_3$ [33], but was not observed in another report [5]. We did not observe any anomalous behavior at these temperatures. However, this effect may be beyond the sensitivity of our measurement for a polycrystalline sample, where anisotropic effects are averaged out. On the other hand, if dense hexagonal $RMnO_3$ materials are prone to slight non-stoichiometric behavior on heating due to slow kinetics, as seen here in the temperature range 400–600 °C, unusual changes of lattice constants could be due to CE associated with the reduction of a slightly oxygenated sample to stoichiometric oxygen content.

The CE during transition from the $Hex_2/P6_3cm$ mixed state (~85/15%, $\delta\approx0.22$) material to nearly single phase $P6_3cm$ has a larger effect on total expansion than TE. Clearly, the CE value is not significantly affected by thermal expansion in the 300–380 °C temperature range. As discussed previously, the primary cause of the CE seen here is due to the change of ionic radius of the $Mn^{(3+2\delta)+}$ cation. Significantly, the CE value of the $Hex_2/P6_3cm$ transition is of the same order of magnitude as the CE associated with the absorption and desorption of oxygen from stoichiometric perovskite $LaMnO_3$ and various substituted perovskite materials ($\sim2.4\times10^{-2}\,mol^{-1}$ and ~1–$4\times10^{-2}\,mol^{-1}$) [34–36]. However, the effect of CE in the hexagonal structure is much more prominent than in the perovskite phase, due to the larger change in oxygen content occurring over a much narrower temperature range.

4. Conclusions

Our synthesis results and previous work with perovskite manganites suggest that formation of the hexagonal $DyMnO_{3+\delta}$ phase under reducing conditions and, by the same argument, previous reports of formation of the perovskite phase with smaller rare-earths (Ho, Er, and Y) under high-pressure, are the result of the tolerance factor's dependence on temperature, oxygen content, and compressibility of the (R–O) and (Mn–O) bonds. Annealings in air and oxygen at ~300 °C of the $P6_3cm$ hexagonal phase yielded unusually high increases of oxygen content, and XRD and TGA measurements indicate two new stable hexagonal $DyMnO_{3+\delta}$ phases in this system for $\delta=0.25$ (Hex_2) and $\delta\approx0.4$ (Hex_3). Rietveld refinements of neutron and synchrotron diffraction data of the Hex_2 phase strongly suggest it is well modeled by the $R3$ space group. Both the Hex_2 and Hex_3 phases are currently being investigated with further NPD measurements with other related hexagonal manganites. TGA and XRD measurements of these new phases show a sharp transition back to the stoichiometric $P6_3cm$ phase above ~350 °C and decomposition back to the perovskite phase above ~1100 °C in O_2. The TEC of the Hex_2 and the $P6_3cm$ phases were determined to be quite different, 11.6×10^{-6} and $2.1\times10^{-6}\,K^{-1}$, respectively, and the chemical expansion of $3.48\times10^{-2}\,mol^{-1}$ associated with the transition between these phases was found to be similar to

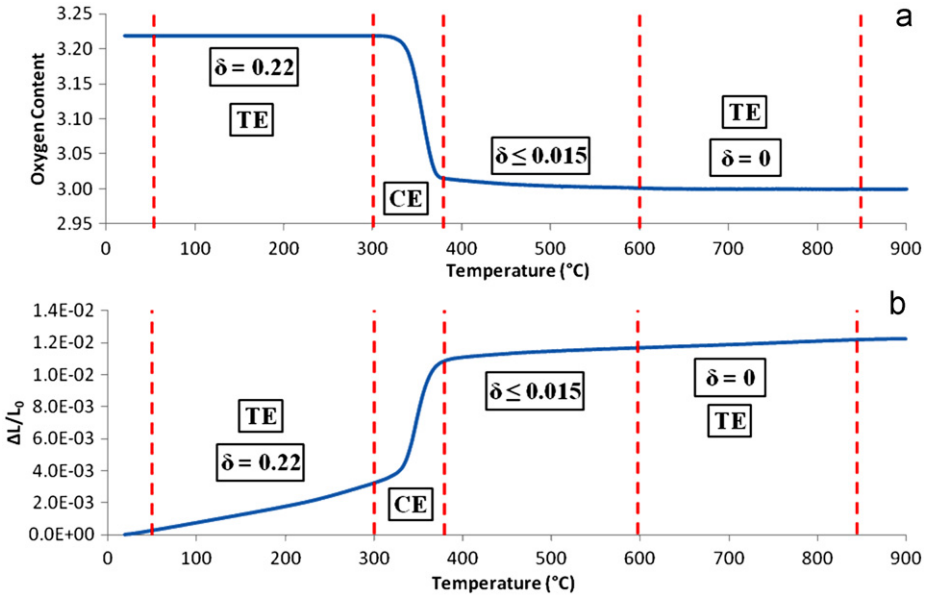

Fig. 9. (a) Dilatometry measurement of hexagonal $DyMnO_{3+\delta}$ in 21% O_2 and (b) TGA measurement of hexagonal $DyMnO_{3+\delta}$ in 21% O_2.

perovskite materials. Strong oxygen content dependence of the structural properties of $DyMnO_{3+\delta}$ suggest that other properties, for example, magnetic and ferroelectric, may change significantly with oxygen content for $DyMnO_{3+\delta}$, as well as for other hexagonal $RMnO_{3+\delta}$ manganites.

Acknowledgments

We would like to thank Prof. Leopoldo Suescun (Cryssmat-Lab/Detema, Facultad de Química, Universidad de la República) for his preliminary structural work and Stephen Boona and Donald Johnson for their laboratory support at Northern Illinois University. This work was supported by the U.S. DOE under Contract no. DE-AC02-06CH11357. Work at PAS was supported by the Polish Ministry of Science and Higher Education from funds for science for 2008–2011 years, as a research project (2047/B/H03/2008/34).

References

[1] H.L. Yakel, W. Koehler, E. Bertaut, E. Forrat, Acta Crystallogr. 16 (1962) 957.
[2] J.B. Goodenough, Phys. Rev. 100 (1955) 564.
[3] J.S. Zhou, J.B. Goodenough, Phys. Rev. B 68 (2003) 144406.
[4] B. Dabrowski, S. Kolesnik, A. Baszczuk, O. Chmaissem, T. Maxwell, J. Mais, Solid State Chem. 178 (2005) 629.
[5] T. Katsufuji, M. Masaki, A. Machida, M. Moritomo, K. Kato, E. Nishibori, M. Takata, M. Sakata, K. Ohoyama, K. Kitazawa, H. Takagi, Phys. Rev. B 66 (2002) 134434.
[6] J.S. Zhou, J.B. Goodenough, J.M. Gallardo-Amores, E. Morán, M.A. Alario-Franco, R. Caudillo, Phys. Rev. B 74 (2006) 014422.
[7] M. Fiebig, T. Lottermoser, R.V. Pisarev, Appl. Phys. 93 (2003) 8194.
[8] O.P. Vajik, M. Kenzelmann, J.W. Lynn, S.B. Kim, S.W. Cheong, Phys. Rev. Lett. 94 (2005) 087601.
[9] Th. Lonkai, D.G. Tomuta, U. Amann, J. Ihringer, R.W.A. Hendrikx, D.M. Többens, J.A. Mydosh, Phys. Rev. B 69 (2004) 134108.
[10] I. Jeong, N. Hur, T. Proffen, Appl. Crystallogr. 40 (2007) 730.
[11] C.N.R. Rao, C.R. Serrao, Mater. Chem. 17 (2007) 4931.
[12] W.S. Choi, D.G. Kim, S.S.A. Seo, S.J. Moon, D. Lee, J.H. Lee, H.S. Lee, D.Y. Cho, Y.S. Lee, P. Murugavel, J. Yu, T.W. Noh, Phys. Rev. B 77 (2008) 045137.
[13] S. Nandi, A. Kreyssig, J. Yan, M. Vannette, J. Lang, L. Tan, J. Kim, R. Prozorov, T. Lograsso, R. McQueeny, A. Goldman, Phys. Rev B 78 (2008) 075118.
[14] S. Harikrishnan, S. Rößler, C.M. Naveen Kumar, H.L. Bhat, U.K. Rößler, S. Wirth, F. Steglich, S. Elizabeth, Phys. Condens. Matter 21 (2009) 096002.
[15] S. Nandi, A. Kreyssig, J.Q. Yan, M.D. Vannette, J.C. Lang, L. Tan, J.W. Kim, R. Prozorov, T.A. Lograsso, R.J. McQueeney, A.I. Goldman, Phys. Rev. B 78 (2008) 075118.
[16] V.Y. Ivanov, A.A. Mukhin, A.S. Prokhorov, A.M. Balbashov, L.D. Iskhakova, Phys. Solid State 48 (2006) 1726.
[17] N. Kamegashira, H. Satoh, S. Ashizuka, Mater. Sci. Forum 449 (2004) 1045.
[18] R.D. Shannon, Acta Crystallogr. A 32 (1976) 751.
[19] H.L. Yakel, Acta Crystallogr. 8 (1955) 394.
[20] H.L. Yakel, W.C. Koehler, E.F. Bertaut, E.F. Forrat, Acta Crystallogr. 16 (1963) 957.
[21] M.A. Subramanian, C.C. Torardi, D.C. Johnson, J. Pannetier, A.W. Sleight, Solid State Chem. 72 (1988) 24.
[22] B. Dabrowski, O. Chmaissem, J. Mais, S. Kolesnik, J.D. Jorgensen, S. Short, Solid State Chem. 170 (2003) 154.
[23] C. Larson, R.B. Von Dreele, Los Alamos National Laboratory Reports LAUR, 1994, pp. 486–748.
[24] O. Carp, L. Patron, A. Ianculescu, J. Pasuk, R. Olar, J. Alloys Compd. 351 (2003) 314.
[25] G. Szabo, R.A. Paris, Seances Acad. Sci. C 268 (1969) 517.
[26] H.W. Brinks, H. Fjellvág, A. Kjekshus, Solid State Chem. 129 (1997) 334.
[27] L. Suescun, B. Dabrowski, J. Mais, S. Remsen, J.W. Richardson Jr., E.R. Maxey, J.D. Jorgensen, Chem. Mater. 4 (2008) 1636.
[28] S. Remsen, B. Dabrowski, J. Mais, unpublished data.
[29] B. Dabrowski, P.W. Klamut, Z. Bukowski, R. Dybzinski, J.E. Siewenie, Solid State Chem. 144 (1999) 461.
[30] Z. Bukowski, B. Dabrowski, J. Mais, P.W. Klamut, S. Kolesnik, O. Chmaissem, Appl. Phys. 9 (2000) 5031.
[31] I.O. Troyanchuk, A.I. Akimov, L.A. Bliznjuk, N.V. Kasper, J. Alloys Compd. 228 (1995) 83.
[32] J. Rodríguez-Carvajal, M. Hennion, F. Moussa, A.H. Moudden, L. Pinsard, A. Revcolevschi, Phys. Rev. B 57 (1998) R3189.
[33] H.D. Zhou, J.C. Denyszyn, J.B. Goodenough, Phys. Rev. B 72 (2005) 224401.
[34] X. Chen, J. Yu, S.B. Adler, Chem. Mater. 17 (2005) 4537.
[35] S. Miyoshi, J. Hong, K. Yashiro, A. Kaimai, Y. Nigara, K. Kawamura, T. Kawada, J. Mizusaki, Solid State Ionics 161 (2003) 209.
[36] S. McIntosh, J.F. Vente, W.G. Haije, D. Blank, H. Bouwmeester, Chem. Mater. 18 (2006) 2187.
[37] S. Pei, M. Kleefisch, T. Kobylinski, J. Faber, C. Udovich, V. Zhang-McCoy, B. Dabrowski, U. Balachandran, R. Mieville, R. Poeppel, Catal. Lett. 30 (1994) 201.
[38] A. Atkinson, T. Ramos, Solid State Ionics 129 (2000) 259.
[39] J. Van Roosmalen, E. Cordfunke, R. Helmhodt., H. Zandbergen, Solid State Chem. 110 (1994) 100.